J Therm Anal Calorim (2013) 111:1107–1119
DOI 10.1007/s10973-012-2269-7

Synthesis and characterization of zinc oxide nanoparticles

Application to textiles as thermal barriers

Narcisa Vrinceanu · Diana Tanasa · Claudia Mihaela Hristodor · Florin Brinza · Eveline Popovici · Daniel Gherca · Aurel Pui · Diana Coman · Andreea Carsmariu · Ionut Bistricianu · Gianina Broasca

CEEC-TAC1 Conference Special Issue

Abstract The research is aimed at synthesis and characterization of nanoscaled zinc oxide particles and their application on linen fibrous supports, for thermal properties. To impart thermal activity to the fibrous nanocomposites, nanoparticles as well as fibrous nanocomposites were produced in different hydrothermal conditions of temperature (90 °C). To characterize the nanoparticles composition, their shape, size, and crystallinity, investigations technique, such as Fourier transformed infrared spectroscopy, scanning electron microscopy, and X-ray powder diffractometry were used. Differential scanning calorimetry analysis profiles were also revealed. The thermal treatment of linen fabrics with nanosized ZnO does not modify significantly their thermal stability.

Keywords Zinc oxide nanoparticles · Thermal barrier · Fibrous support · Crystallinity · Calorimetry · Spectroscopy · Diffractometry · Microscopy

N. Vrinceanu · D. Tanasa · C. M. Hristodor (✉) · F. Brinza · E. Popovici · D. Gherca · A. Pui
Alexandru Ioan Cuza University, 11 Bulevard Carol I, 700506 Iasi, Romania
e-mail: hristodorc@yahoo.com

N. Vrinceanu · D. Coman
Lucian Blaga University, 2-4 Ion Ratiu Street, 500215 Sibiu, Romania

A. Carsmariu · I. Bistricianu · G. Broasca
Gheorghe Asachi Technical University, 53 Mangeron Street, 7000205 Iasi, Romania

Introduction

The degradation of polymeric materials is caused by exposure to various factors such as heat, UV light, irradiation ozone, mechanical stress, and microbes. Degradation is promoted by oxygen, humidity and strain, and results in such flaws as brittleness, cracking, and fading [1]. There have been research reports targeting nanosized magnetic materials synthesis, having significant potential for many applications [2–5].

ZnO particles have been applied for varistors and other functional devices, and also can be used as reinforcement phase, wear resistant phase, and anti-sliding phase in composites in consequence of their high elastic modulus and strength. Otherwise, ZnO particles exist in anti-electrostatic or conductive phase due to their current characteristics [6–8]. Few studies have been concerned with the application of ZnO nanoparticles in coatings system with multi-properties. The nanocoatings can be obtained by the traditional coatings technology, i.e., by filling with nanometer-scale materials.

Both structure and functional properties of coatings can be modified by filling with nanomaterials. Super-hardness, wear resistant, heat resistance, corrosion resistance, and about function, anti-electrostatic, antibacterial, anti-UV and infrared radiation all or several of them can be realized [9–12].

The aim of this study was to study the thermal degradation behavior of some textile nanocomposites made of nano/micron particle grade zinc oxide and linen fibrous supports, and to discuss the thermal degradation mechanism of the above mentioned structures. Second, the objective of the research was to investigate the effect of the functionalization agent—monochlorotriazinyl-β-cyclodextrin (MCT-β-CD) on the thermal stability and degradation

mechanism of ZnO-nanocoated linen fibrous samples. To improve the thermal stability of the fibrous nanocomposites, montmorillonite (MMT) emulsion was applied on the supports, before the ZnO coating.

Montmorillonite (MMT) is a type of inorganic natural clay which has silicate (SiO_4) tetrahedral sheets arranged into a two-dimensional network structure [13]. MMT can provide thermal resistance, wrinkle resistance, and antibacterial properties on textiles [14–19].

Throughout the study, the particle sizes of the MMT were reduced by an ultrasonic crashing machine. The reduced particles in an emulsion form were padded onto the linen fibrous samples.

The instrumental methods were conducted to measure the particle sizes of the reduced zinc oxide particles to characterize the surface morphology and chemical composition of the treated supports. The understanding of the thermal behavior of these fibers is very important as in general several conventional techniques used in textile processing industry are conducted at high temperature.

Experimental

Materials

Two 100% twill linen supports, each of size 3 × 3 cm. The supports had been desized, scoured, and bleached. One of the supports has been coated with a certain concentration of MCT-β-CD. The MCT-β-CD under the trade name CAVATEX or CAVASOL® W7 MCT (CAVATEX) was purchased by the company Wacker Chemie AG. The product does not irritate nor initiates sensitization and is an effective tool to modify textile surfaces [20].

Determination of the concentration of dispersing agent for preparing the MMT emulsion

Bentonite montmorillonitic clay (MMT) was provided by firma Riedel-de Haen Chemicals Company. Given the compositional complexity of clay materials, we considered useful as a first step to perform an ion exchange process, for their cleansing, to reach the transition cations sodium form. The clay exchange in Na^+ form was conducted using a 1 M NaCl solution with a ratio a solid/liquid 1:10.

Preparation of composites

To make composite samples, the particle sizes of the MMT were reduced by an ultrasonic crashing machine. To prepare a good MMT emulsion such that the tiny particles of MMT should be well dispersed and will not be aggregated again to form large molecules, a nonionic dispersing agent, SETAVIN from CLARIANT, was used for dispersing the MMT clay to form an emulsion. The emulsion was prepared by adding 1 g of MMT into 42 mL of dispersing agent. The emulsion was magnetically stirred for 2 h. Then the emulsion was crashed by an ultrasonic crashing machine for 30 min, to reduce the particle sizes. After crashing, the behavior of the emulsion of the dispersing agent was observed carefully at different time intervals, i.e., 5, 10, 15, 30 min.

In addition, a binder resin (from ARALDITE Company) was also prepared. The thus obtained resin solution was carefully poured drop wise. The mixture was then slowly stirred until homogeneous. Subsequently, ZnO nanoparticles emulsion with concentration of 0.5% was added. The resulting composite was allowed to stand overnight to remove air bubbles, before use. The synthesis of this oxide by hydrothermal method has been described elsewhere.

After preparing the MMT–ZnO emulsion, it was padded onto the four different linen fibrous supports:

- Reference linen support (without MCT) and ZnO;
- Linen support with MCT and without ZnO;
- Non-functionalized linen support without MCT and with ZnO;
- Functionalized linen support with MCT and ZnO, using a padding machine.

Due to the poor dispersing properties of the MMT particles, this padding process should be carried out as soon as possible, i.e., not longer than 30 min after finishing the crashing process, to prevent the reduced particles from aggregating again to form larger molecules. The emulsion was padded onto the linen supports by the padder with the pressure of 3 kg/cm^2 and the speed of 5 rpm. Two padding times were investigated including 3 padding times and 6 padding times, and subsequently the wet pick-up was 84.21 and 88, respectively. Finally, the treated fabrics were dried at 140 °C, for 3 min.

Washing was carried out to remove the byproducts. The treated supports were immersed for 5 min in 0.2 g/L sodium lauryl sulfate dodecyl, to remove the unbound nanoparticles. Then the fibrous supports were rinsed at least 10 times to completely take out all the soap solution. The samples thus washed were air dried. Simultaneously, a reference emulsion made by MMT without ZnO was applied for comparison.

Thermal treatment relied into two main stages, into the calcination oven. First, the samples were subjected to an increasing of temperature up to 150 °C; second, the probes were heated up to 350, 450 °C.

Instrumental methods

The instrumental methods were conducted to measure the particle sizes of the ZnO particles to characterize the

surface morphology and chemical composition of the treated supports.

X-Ray diffraction (XRD)

Diffractograms were recorded using a PW1710 diffractometer using Cu-Kα radiation ($k = 1.54$ Å) source (applied voltage 40 kV, current 40 mA). Scattered radiation was detected in the $2\theta = 10$–$80°$ range at a speed of 1.5° min^{-1}.

Evaluation of crystallinity

The extent of crystallinity (I_C) was estimated by means of Eq. 1, where I_{020} is the intensity of the 020 diffraction peak at 2θ angle close to 22.6°, representing the crystalline region of the material, and I_{am} is the minimum between 200 and 110 peaks at 2θ angle close to 18°, representing the amorphous region of the material in cellulose fibers [21–23]. I_{020} represents both crystalline and amorphous materials while I_{am} represents the amorphous material.

$$I_C = \frac{I_{020} - I_{am}}{I_{020}} \times 100\,(\%). \quad (1)$$

A *shape factor* is used in X-ray diffraction to correlate the size of sub-micrometre particles, or crystallites, in a solid to the broadening of a peak in a diffraction pattern. In the Scherrer equation,

$$\tau = \frac{K \cdot \lambda}{\beta \cos\theta},$$

where K is the shape factor, λ is the X-ray wavelength, β is the line broadening at half the maximum intensity (FWHM) in radians, and θ is the Bragg angle [24]. τ is the mean size of the ordered (crystalline) domains, which may be smaller or equal to the grain size. The dimensionless shape factor has a typical value of about 0.9, but varies with the actual shape of the crystallite. The Scherrer equation is limited to nanoscale particles.

Surface morphology

The surface morphology of the MMT-treated was investigated by scanning electron microscope (SEM) Quanta 200 3D Dual Beam type microscope, from FEI Holland, coupled at a EDS analysis system manufactured by EDAX-AMETEK Holland equipped with a SDD type detector (silicon drift detector) with magnification of 300×, 1200×, respectively. Taking into account the sample type, the analyses have been performed, using low vacuum working mode, allowing the probes testing in their initial state, without a previous metallization (as in high vacuum working type). Both for the acquisition of secondary electrons images (SE—secondary electrons) and EDS type elemental chemical analyses, large field detector (LFD) type detector has been used, running at a pressure of 60 Pa in working room, and a voltage of 30 kV.

Thermal analysis

The differential scanning calorimetry (DSC) analysis of fibrous supports–ZnO composites were carried out using a NETZSCH DSC 200 F3 MAIA instrument under nitrogen. Initial sample weight was set as 30–50 mg for each operation. The specimen was heated from room temperature to 350 °C at a heating rate of 10 °C/min.

IR-spectroscopic analysis

A FTIR JASCO 660+ spectrometer Fourier Transform Infrared Spectrometer operating in the 4,000–400 cm^{-1} range was used to record the IR spectra. The KBr pellet technique was used to prepare the powder samples for IR studies. Film samples were powdered, mixed with KBr, and then pressed into pellets before recording the spectra. The average of three scans for each sample was taken for the peak identification. The characteristic infrared bands of the chemical compounds existed in the studied samples were studied by using a Perkin Elmer System 2000 of Fourier transform infrared spectrophotometer (FTIR) with the scanning range between 4,000 and 450 cm^{-1}.

Results and discussion

Due to unknown causes, the dispersion of the MMT particles was not made in a proper manner onto all four samples; consequently, we proceeded to consider for investigation only the last two samples:

- Non-functionalized linen support without MCT and with ZnO, with the assistance of MMT;
- Functionalized linen support with MCT and ZnO, with the assistance of MMT (Table 1).

SEM investigations of L1, L2, L3, L/MCT-1, L/MCT-1, and L/MCT-1 are shown in Figs. 1, 2, 3, 4, 5, and 6, respectively.

EDX-elemental analysis is shown in Figs. 7, 8, 9, 10, 11, 12 and Tables 2 and 3, indicating that ZnO nanocomposites contain different percentage content of zinc oxide.

For non-functionalized linen supports set, see Figs. 7, 8, 9.

From the EDX investigation a decreasing of zinc oxide content with the increasing of the treatment temperature is remarkable, for both types of studied samples (Tables 2, 3).

Table 1 Specifications and descriptions of the samples

Sample names	Description
MCT	Monochlorotriazinyl-β-cyclodextrin
MMT	Bentonite montmorillonitic clay
ZnO	ZnO powder hydrothermally synthesized
L1	Non-functionalized linen support without MCT and with ZnO, with the assistance of MMT, thermally non-treated
L2	Non-functionalized linen support without MCT and with ZnO, with the assistance of MMT, treated at 150 °C
L3	Non-functionalized linen support without MCT and with ZnO, with the assistance of MMT, treated at 350 °C
L/MCT-1	Functionalized linen support with MCT and ZnO, with the assistance of MMT, thermally non-treated
L/MCT-2	Functionalized linen support with MCT and ZnO, with the assistance of MMT, treated at 150 °C
L/MCT-3	Functionalized linen support with MCT and ZnO, with the assistance of MMT, treated at 450 °C

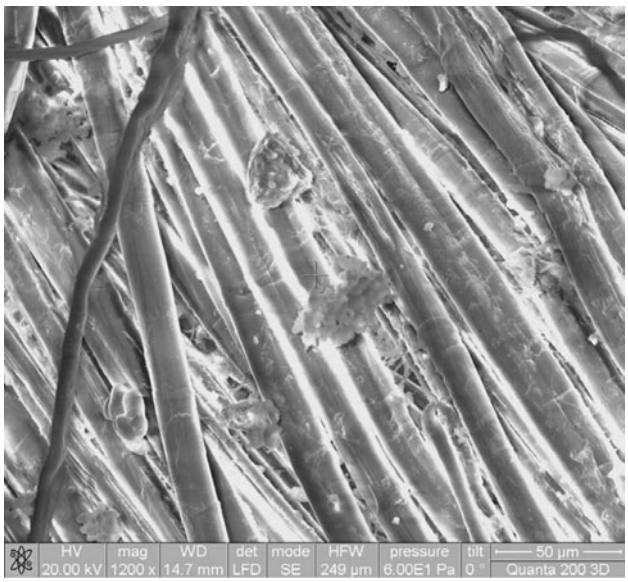

Fig. 1 SEM image for L1

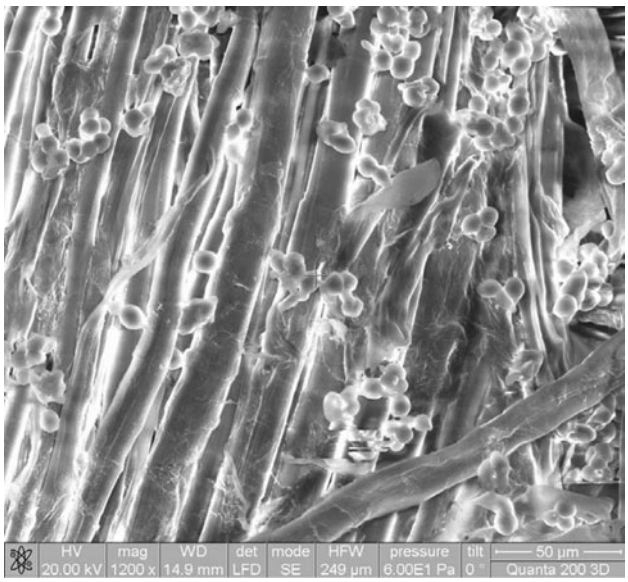

Fig. 3 SEM image for L3

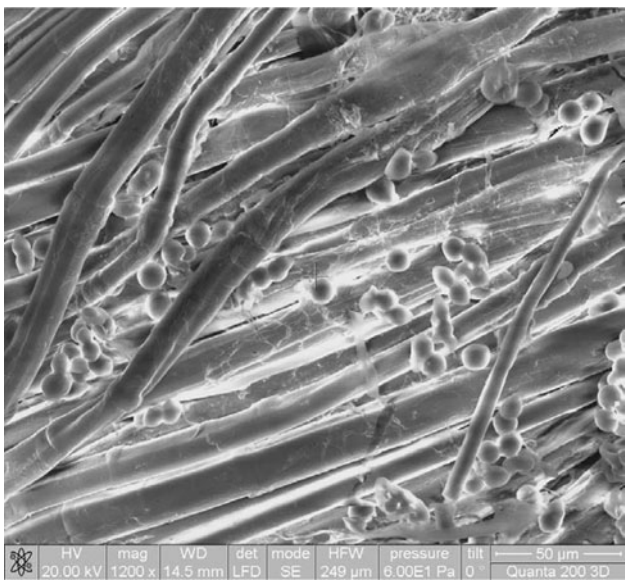

Fig. 2 SEM image for L2

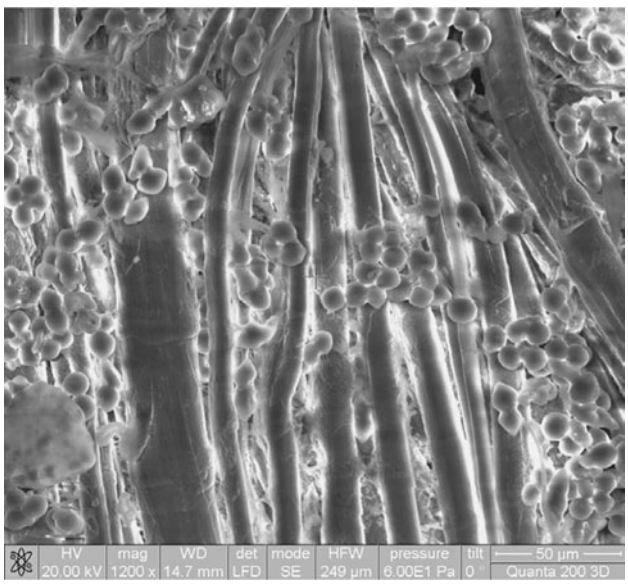

Fig. 4 SEM image for L/MCT-1

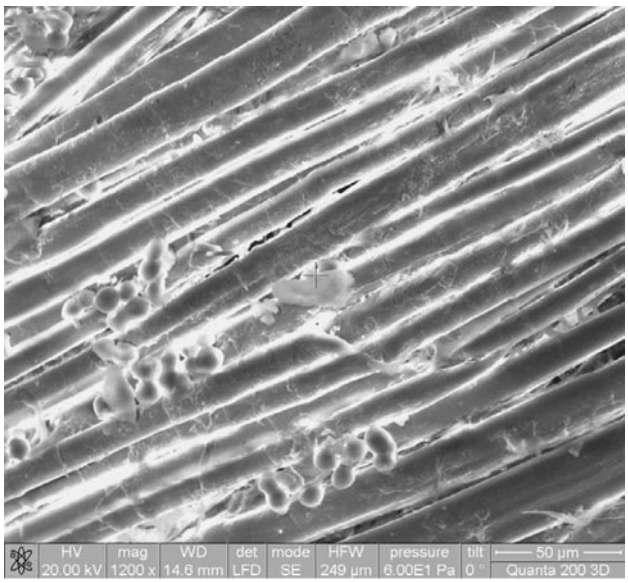

Fig. 5 SEM image for L/MCT-2

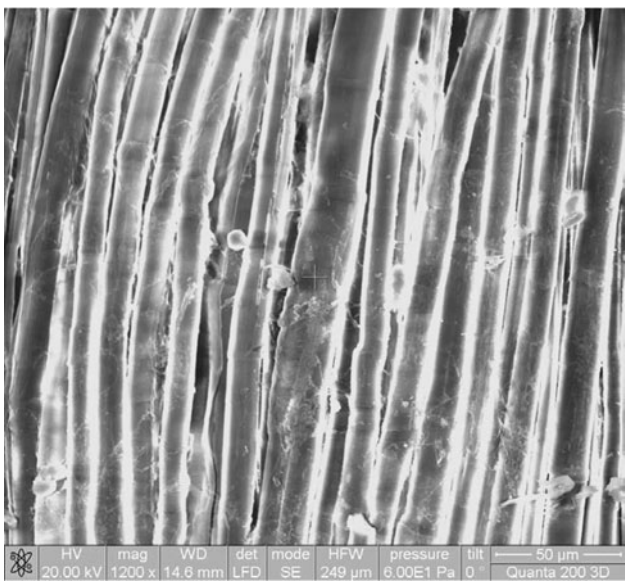

Fig. 6 SEM image for L/MCT-3

From the SEM photos and comparing the morphology of the two types of samples before and after thermal treatment, some randomly distributed conglomerations are noticeable, in case of *non-functionalized sample*, while on the *functionalized linen sample*, the particles have bigger dimensions and uniformly distributed.

In case of *functionalized linen sample* some observations could be done:

– by thermal treatment at 150 °C, the nanoparticels are smaller and partially cover the fiber body (L/MCT-2);

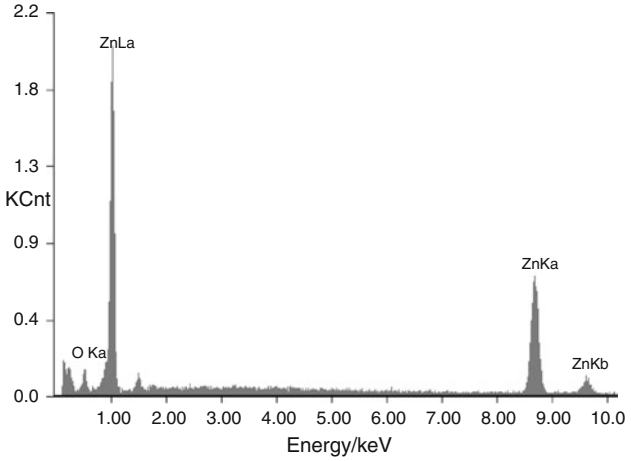

Fig. 7 EDX analysis for L1

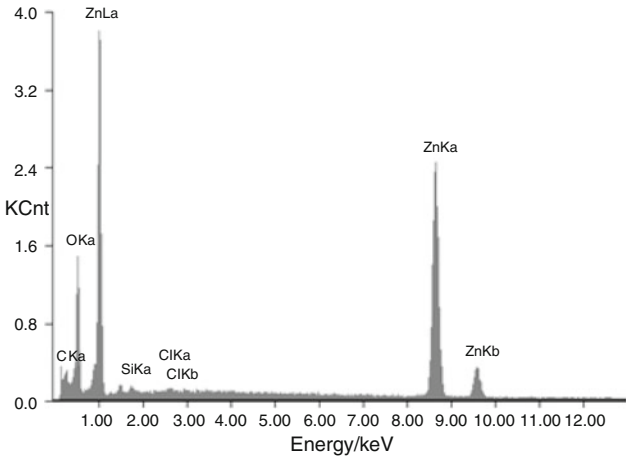

Fig. 8 EDX analysis for L2

– by increasing the temperature of the treatment up 450 °C, the size of the unfixed ZnO nanoparticles increases and the fibers are uniformly coated (L/MCT-3).

In case of *non-functionalized linen support:*

– by thermal treatment up to 150 °C, the nanoparticles sizes randomly augmented (L2);
– at 350 °C thermal treatment, the dimensions of the particles diminished and their distribution is relative uniform (L3).

Concluding, the differences between the morphology of the two studied samples are the following:

The increasing of the temperature induced the increasing of the zinc oxide nanoparticles sizes on the functionalized linen sample. On the contrary, the non-functionalized sample, the dimensions of the nanoparticles decreased.

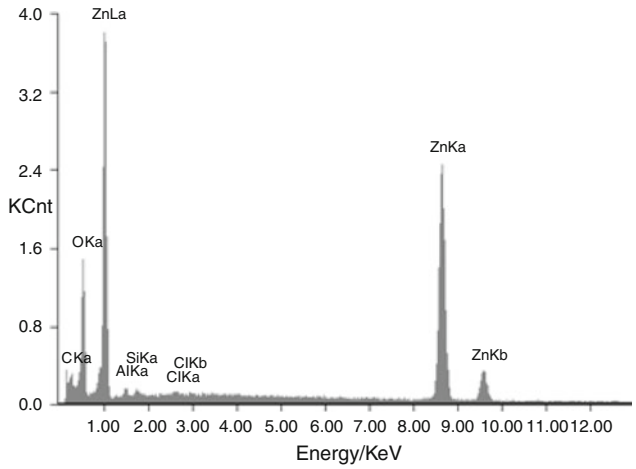

Fig. 9 EDX analysis for L3

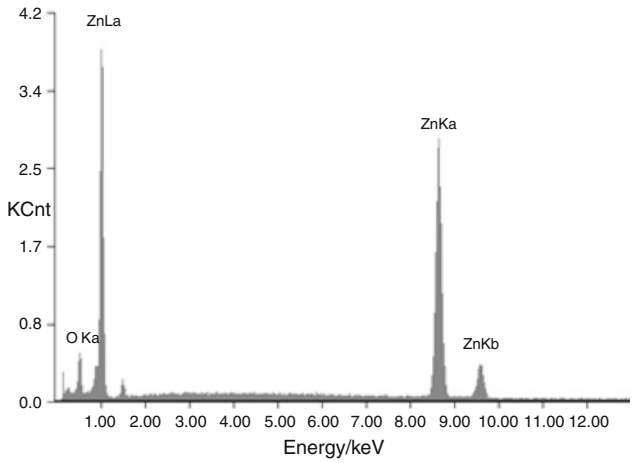

Fig. 11 EDX analysis for L/MCT-2

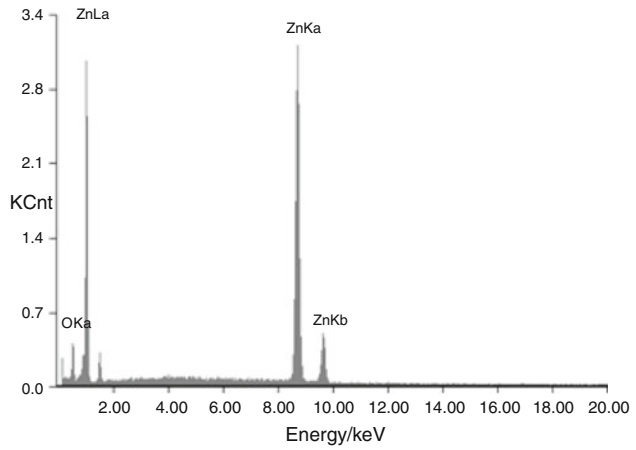

Fig. 10 EDX analysis for L/MCT-1

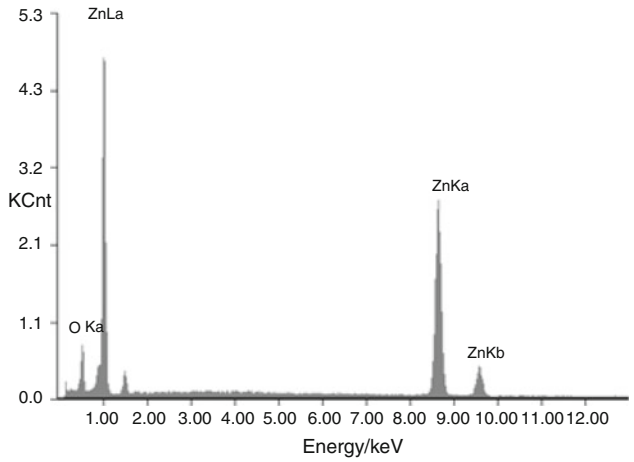

Fig. 12 EDX analysis for L/MCT-3

Generally speaking, there are two processes occurring—the nuclei increasing and their dissolving.

The explanation relies from the fact that consequently to functionalization, crystallization nuclei, strongly adherent, whose augmentation is favoured by temperature increasing, is noticed.

On non-functionalized samples, the adherence of particles is weak, and along with temperature increasing, their destruction took place.

Concluding, EDX analysis revealed a proportional decreasing of ZnO% content with the increasing of thermal treatment.

For XRD patterns interpretation, see Fig. 13.

The XRD patterns exhibit for specific peaks for flax fibers, meaning: four well-defined peaks at 15.1°, 16.8°, 22.0°, and 34.4°, the values of 15.1° and 16.8° for the 2θ reflection, corresponding to the 110 crystallographic planes, respectively (Fig. 13a). The other two peaks at 22.0 and 34.4 correspond to the 002 and 004 planes, respectively, which is in accordance with the literature [24].

In case of the functionalized linen support, three peaks appeared around 15.5°, 22.0°, and 34.4°, corresponding to the 110, 002, and 004 planes, respectively (Fig. 13b), which is due to the large amount of amorphous regions present in cellulose, and also to the presence of amorphous lignin and hemicelluloses, which agrees with the results of Tserki [24, 25].

The peak characteristic to flax fibers (Pos.[°2Th.] ranging between 30° and 40°) seemed to overlap to those specific to both ZnO and MMT. Although more attenuated or less visible, due to the small concentration of the ZnO solution, in our opinion, the peaks could be assigned to ZnO, as well.

In case of L2 sample, it is noticeable that the apex of the peak specific for MMT is also found in the L3, meaning that MMT was not thermally degraded. Moreover, the crystallinity index increased, from a thermal stage to other. Generally, through calcination process, it can be stated that the CI is maintained approximately constant, meaning that

Table 2 Surface composition from EDX measurements

Elements	Wt/%	At/%
OK		
L1	28.91	62.43
L2	27.40	42.74
L3	27.08	42.18
ZnK		
L1	71.09	37.57
L2	54.43	20.78
L3	53.64	20.45
CK		
L1	17.14	35.61
L2		
L3	17.06	35.40
SiK		
L1	00.77	00.68
L2		
L3	00.76	00.67
ClK		
L1		
L2		
L3	00.26	00.18
AlK		
L3	01.2	01.11

Wt weight percent, *At* atomic percent, for samples L1, L2, and L3

Table 3 Surface composition from EDX measurements

Elements	Wt/%	At/%
OK		
L/MCT-1	08.94	28.6
L/MCT-2	12.05	35.89
L/MCT-3	15.35	42.56
ZnK		
L/MCT-1	91.06	71.37
L/MCT-2	87.95	64.11
L/MCT-3	84.65	57.44

Wt weight percent, *At* atomic percent, for L/MCT-1, L/MCT-2, and L/MCT-3

the assistance of MMT before the application by padding of zinc oxide, stabilizes in a certain extent the fibrous support.

Referring to the functionalized type, a more enhanced CI has been obtained, probably due the existence of MCT on the fibrous surface support, playing the role of entrapping/entrapment of the ZnO nanoparticles, as it can be found in a previous study. However, the XRD analysis revealed the fact that the entrapment was not good enough. This can be explained also by the fact that the repeated

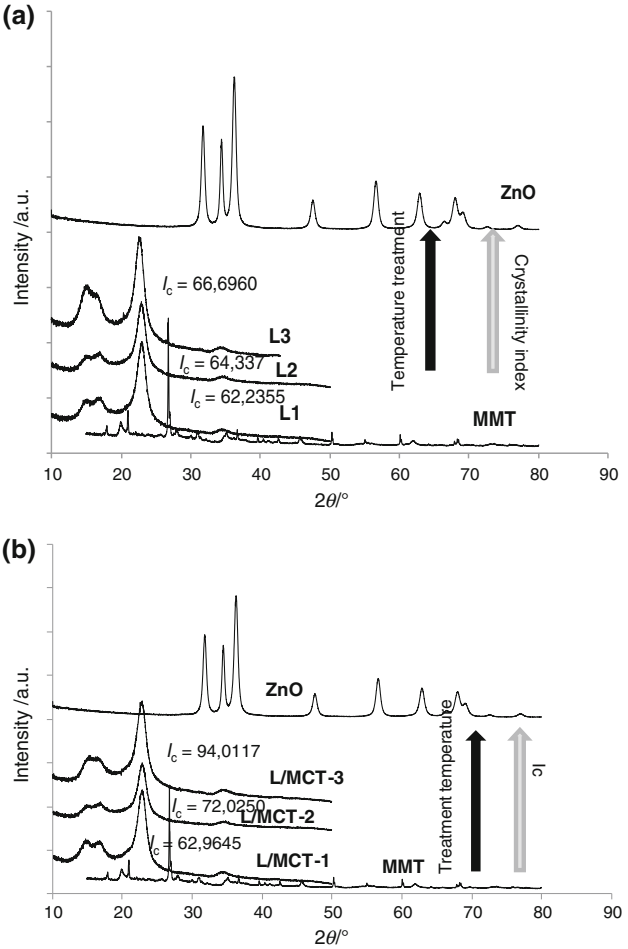

Fig. 13 XRD patterns of **a** MMT, ZnO, L1, L2, and L3 and **b** L/MCT-1, L/MCT-2, and L/MCT-3

cycles of washing and rinsing conducted to remove the byproducts, contributed also to the washing away of the ZnO unbound particles.

According to [26, 27], a correlation between crystallite size and CI should be done, to generate a clear overview regarding the crystallinity of the studied supports and their novel nanoscale pattern surface achieved by the last being responsible of the thermal protection/barrier.

The *d* spacing of the (020) planes is listed in Table 4 for the two different specimens. Values of *d* for three-non-functionalized linen support with ZnO thermally non-treated and four-functionalized linen support with ZnO treated at 150 °C were almost equal. However, the spacing becomes larger for the three-non-functionalized linen support with ZnO treated at 150 °C and still larger for four-functionalized linen support with ZnO thermally non-treated. Changes in the crystallinity index and in the size of the crystals perpendicular to the (020) plane follow a reversed tendency. Spacings of more than 0.4 nm for the (020) planes as shown in Table 4, correspond generally to

Table 4 Correlation between crystallite size and CI

Sample	Crystallite size perpendicular to the (020) planes, by XRD measurement/nm	*d* Spacing of the (020) planes distance/Å	CI/ crystallinity index
L1	10.08	0.3889	0.622
L2	10.32	0.8786	0.643
L3	10.62	0.3928	0.669
L/MCT-1	26.74	0.9060	0.6296
L/MCT-2	11.92	0.387	0.7202
L/MCT-3	10.96	0.3929	0.9401

cellulose microfibrils of low crystallinity and small lateral size, as seen in Table 2, which contrasts with the high crystallinity and large size of the cellulose microfibrils contained in the cell wall. The least crystalline specimens are obviously more distorted, which results in a looser packing of the chains and hence larger unit cell dimensions. After conversion to cellulose I1 by mercerization, crystallinity index and crystal size tend toward similar values for all the celluloses as shown in Table 2. The crystallinity index for the L1, L2, and L3 specimens remains in a narrow range of 0.622–0.669 while it varies from 0.6296 to 0.9401 for the functionalized fibrous linen supports. The crystal size severely decreases for L/MCT-1, L/MCT-2, and L/MCT-3 at the first stage of thermal treatment from 26.74 to 10.96 nm, while it varies from 10.08 to 10.62 nm in non-functionalized linen support through the treatment temperature increasing. There is thus an evident convergence of the crystallinity and of the crystal size during the thermal treatment. These results indicate clearly that in non-functionalized sample of low crystallinity, the summative effect of ZnO, MCT occurrence and the progressive augmentation of the temperature induced a slow increasing of crystallinity and crystal size, while for functionalized specimen, a synergic result occurred: the crystallinity index remarkably increased, and also the crystallite size. We assume that these trends would not be expected without the influence of the chemicals assistance: MCT as functionalization agent, on one hand, and ZnO as stabilizer, on the other hand. These results are more in line with the idea that the efficiency of ZnO particles coating onto previously functionalized linen supports involves an obvious enhanced crystallinity. On the other side, the non-functionalized specimen show a slight improvement of the crystallinity, due the existence of the ZnO nanoparticles, but the absence of the agent of entrapment, the crystallinity is not complete. And this concept is compatible with the data interpretation provided by FTIR analysis. Obviously, we have no definitive proof that the picture presented is correct. However, as far as the authors are aware, this article is the first report that larger crystals and higher crystallinity may be obtained by the synergic assistance of MCT as functionalization agent and ZnO, as thermal barrier conferring compound.

From Table 4 the following can be observed:

- At L/MCT-2, L/MCT-2, and L/MCT-3 specimens, CI increases with the decreasing of the crystallites nanoparticles;
- In case of L1, L2, and L3, there is a proportional increasing of CI with the augmentation of nanoparticles size.

Weak points of the research

CI was calculated from the ratio of the height of the 002 peak (I_{020}) and the height of the minimum (I_{am}) between the 020 and the 101 peaks, as shown in Fig. 13 [28]. This method is useful for comparing the relative differences between samples; however, we suggest that it should not be used as a method for estimating the amount of crystalline and amorphous material in a cellulose sample for the following reasons. (1) The minimum position between the 002 and the 101 peaks (I_{am} which is at about 18.3° in Fig. 13a) is not aligned with the maximum height of the amorphous peak. The apex of the peak that is due to amorphous cellulose is likely to be higher than 18.3°. From the peak deconvolution method, the amorphous peak was predicted to be at around 21.5°. Thus, the I_{am} value for the height method is significantly underestimated, resulting in an overestimation of the CI.

There are at least four crystalline peaks, but only the highest peak (002) is used in the calculation. This fact excludes contributions from the other crystalline peaks, putting too much emphasis on the contribution from one alignment of the cellulose crystal lattice. Peaks in the cellulose diffraction spectrum are very broad and vary considerably in their width. A simple height comparison cannot be expected to provide a reasonable estimate of cellulose crystallinity, as it neglects variation in peak width, which can also be affected by crystallite size [29].

We believe that for these reasons the relative height to the minimum can only be taken as a rough approximation of the contribution of amorphous cellulose to the cellulose diffraction spectrum.

Consequently, comparing the two sets of probes, the functionalized set has CI higher, meaning an improved crystallinity; however, the non-functionalized one revealed also an augmentation of the crystallinity, but a reduced one. The perspective research will be oriented to more improved technique of fixing the ZnO nanoparticles to achieve/add multifunctionality of the studied fibrous nanocomposites.

Thermal degradation of linen fibrous supports treated with ZnO

As the results provided by the XRD analysis are not very relevant, they can be completed, correlated with the DSC studies, as the last type of investigation is able to evaluate the crystallization/melting processes.

The DSC curves of fibrous supports–ZnO nanocomposites under nitrogen are shown in Figs. 14, 15.

In a typical DSC curve of cellulosic fibers, there is generally an endothermic peak in the range 370–395 °C, which has been shown to be primarily due to the production of laevoglucosan [30]. In the case of linen fibers, this peak is sometimes partly or completely marked by an

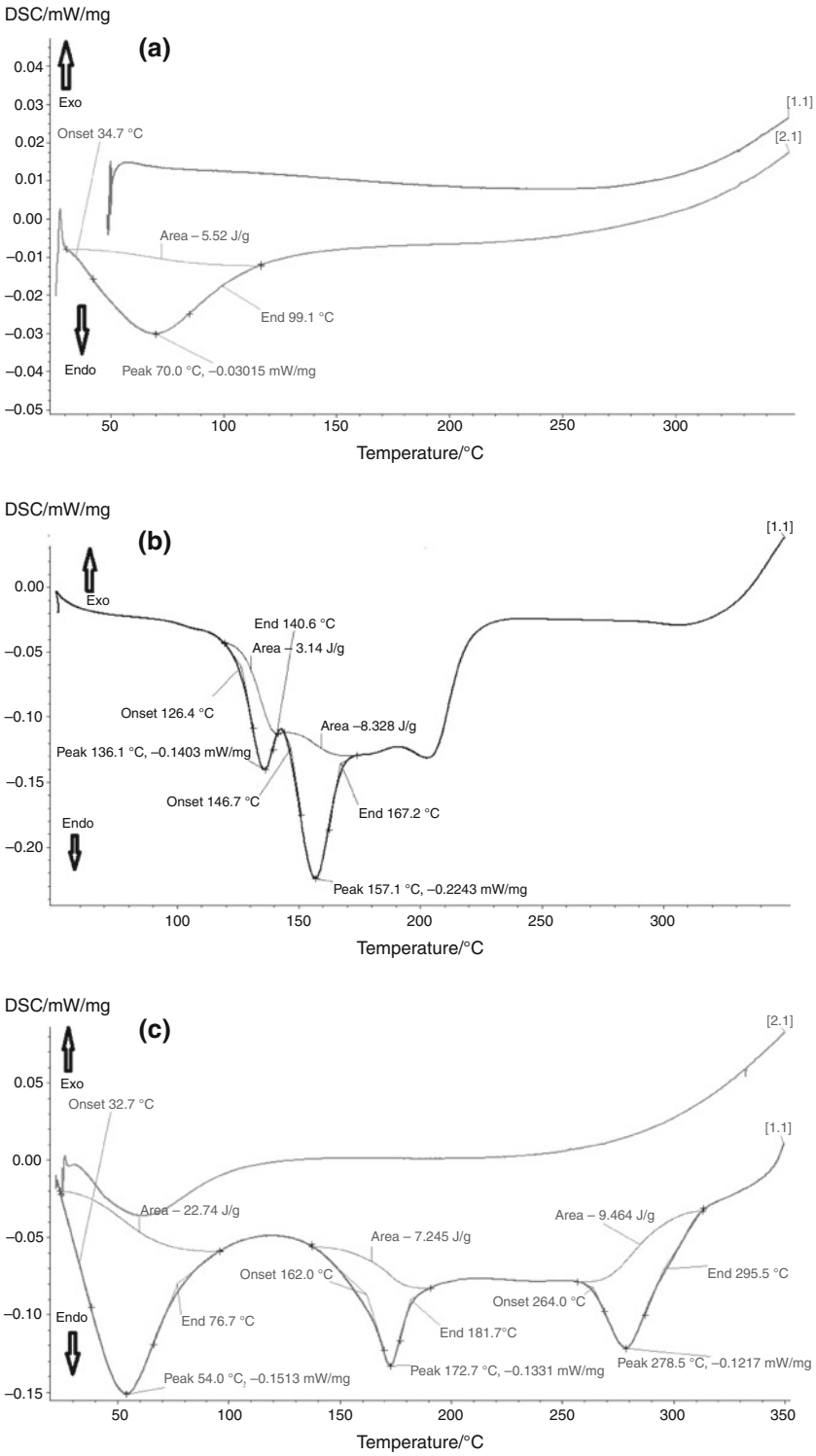

Fig. 14 Typical DSC curve under nitrogen for **a** L1, **b** L2, and **c** L3

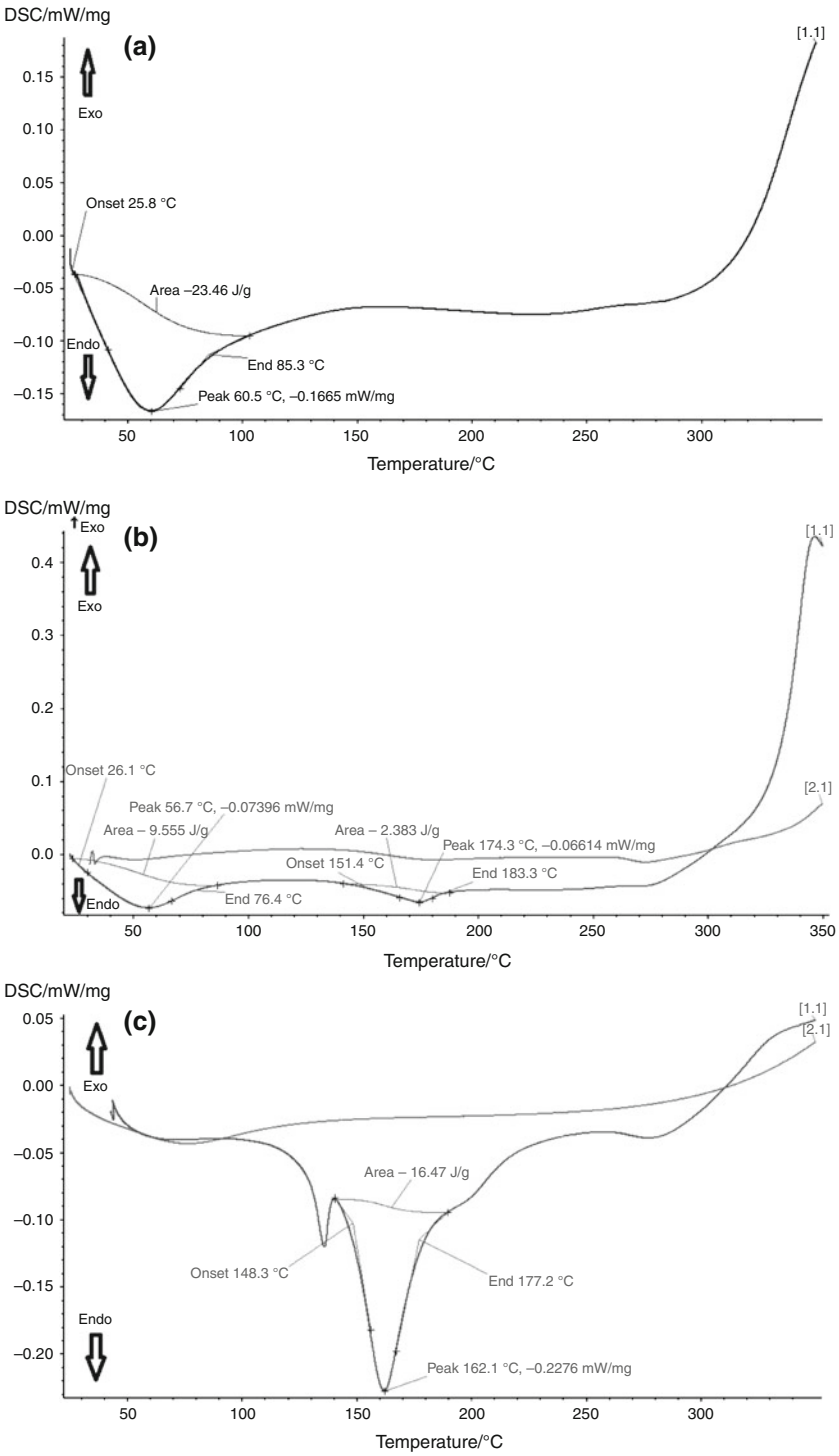

Fig. 15 Typical DSC curve under nitrogen for **a** L/MCT-1, **b** L/MCT-2, and **c** L/MCT-3

exothermal effect around 340 °C, attributed to a base-catalyzed-dehydration reaction that takes place in the presence of alkaline ions, such as those of sodium [31].

A progressive mass loss was observed from 200 to 250 °C associated with water release. It is well known from the literature that lignocellulosic fibers degrade in several steps. The hemicellulose degrades at about 240–310 °C, whereas the cellulose degrades between 310 and 360 °C and the lignin has been shown to degrade in wide temperature interval (200–550 °C) [32]. It is not possible to separate the different degradation processes of the fiber components because the reactions are very complex and overlap in the range of 220–360 °C. It is remarkable that the nanocomposite treated with ZnO nanoparticles with the

assistance of MMT started to decompose at higher temperature than sample treated in the same conditions but without the presence of zinc oxide. However, the existence of the montmorillonitic clay on the surface of the probes delayed the thermal degradation of the fibrous linen samples, even the non-treated with the zinc oxide particles.

It is suggested that cellulose is thermally decomposed through two types of reactions. At lower temperatures, there is gradual degradation which includes dehydration, depolymerisation, oxidation, evolution of carbon monoxide and carbon dioxide, and formation of carbonyl and carboxyl groups, ultimately resulting in carbonaceous residue forms.

The DSC curves in Fig. 14a, b show an endothermic band around 260 °C, indicating a weight loss. In Fig. 14a, as the temperature rises to 310 °C, the surface acidity of zinc oxide nanoparticles keeps accelerating the decomposition of the fibrous substrate. Thus, a very much lower amount of carbonyl groups is found in the linen–ZnO nanocomposite specimens, according to the FTIR spectra.

In the meantime, MMT having a higher thermal conductivity as well as a greater heat capacity value absorb the heat transmitted from the surroundings and retard the direct thermal impact to the polymer backbone [33, 34]. As a result, zinc oxide stabilizes the polymer molecules of the underneath substrates and delays the occurrence of major cracking up to 400 °C (Fig. 15).

The behaviour of the reference fibrous linen (non-functionalized) subjected to the thermal treatment in N_2 clearly shows the masking effect of an exothermal reaction on the endothermic cellulose decomposition.

The sample shows an exothermal peak at 260 °C with a decreased enthalpy after the thermal treatment; the exothermal effect is attributable to β-cellulose decomposition as observed in a curve of a cotton sample.

Surprisingly, even within the second cycle of thermal treatment, the sample exhibits a similar exothermal peak at 363 °C.

For FTIR spectra interpretation, see Fig. 16.

The change of IR spectra (Fig. 16) of the nanocomposite upon heating shows the catalytic effect of ZnO.

The absorption band occurred in all the spectra at 3,450 cm^{-1} wavenumber, corresponding to bond O–H (intermolecular hydrogen bond) vibration.

The absorption bands having a *shoulder* shape present in spectra at about 2,914 and 2,829 cm^{-1} wavenumbers corresponded to the methylene and methyl asymmetrical and symmetrical C–H stretching of aliphatic groups. The sharpness of these two bands is attributed to the low (weak) well-ordered, hydrocarbon chain.

The absorption band from 1,636 cm^{-1} can be assigned to C=C, aldehydic, and carboxyl stretching vibrations. The 1,335–1,316 cm^{-1} doublet is assigned to the cellulose component.

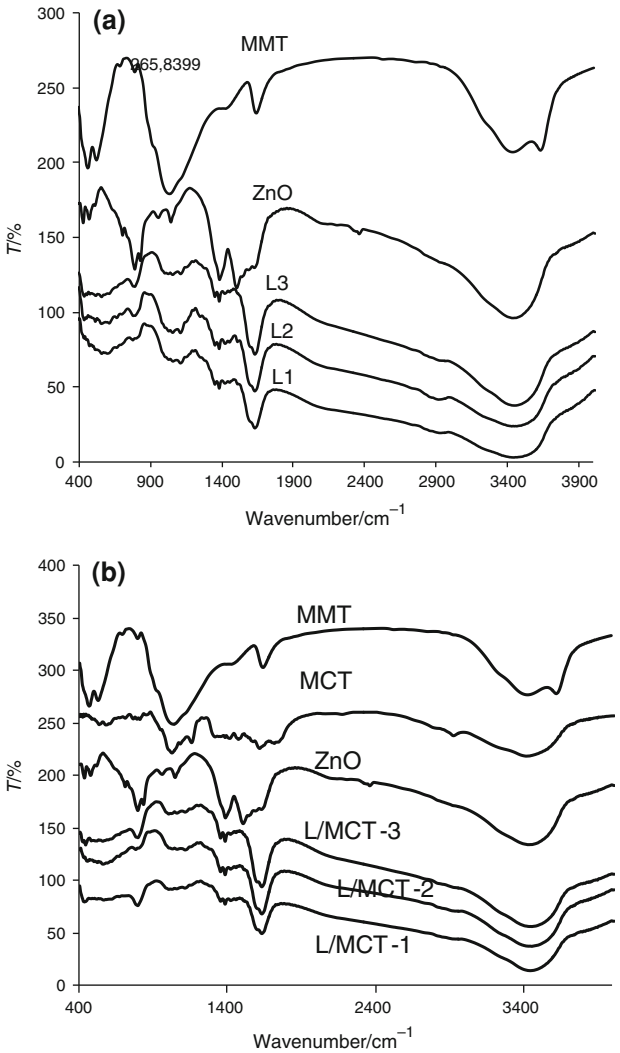

Fig. 16 FTIR spectra for **a** MMT, ZnO, L1, L2, and L3 and **b** L/MCT-1, L/MCT-2, and L/MCT-3

The absorption bands present at 1,115 cm^{-1} are related to the vibration stretching mode C–O.

The deformation beyond the double bond plan from the lateral catena is highlighted in spectra, by bands occurrence at 790 cm^{-1}.

In spectra specific to montmorillonite, a band occurred at 3,700 cm^{-1}, which could be assigned to non-hydrogen bonded O–H stretching vibration (Fig. 16b). As a subsequence of zinc ions in the reaction medium, the intermolecular association process is affected through the hydrogen bonds belonging to OH groups, as the zinc source (precursor) reacted with these groups, forming crystallization nuclei of zinc oxide.

Concluding, the existence of ZnO nanoparticles prevents intermolecular hydrogen bonding, and therefore, the vibrational stretching modes of free O–H appear at a higher wave number.

Conclusions

The study emphasized the ideas of:

- a novel preparing technique to obtain nanoscale ZnO-coated fibrous composites, by using the synergic effect of MMT and MCT;
- the thermal stability and degradation mechanism of ZnO-nanocoated linen fibrous samples;
- cumulative barrier attributes conferred by the two new components that interfered in the preparation techniques: MMT and MCT.

From the SEM photos and comparing the morphology of the two types of samples before and after thermal treatment, some randomly distributed conglomerations are noticeable, in case of *non-functionalized sample*, while on the *functionalized linen sample*, the particles have bigger dimensions uniformly distributed.

EDX investigation highlighted a decreasing of zinc oxide content with the increasing of the treatment temperature, for both the studied samples.

However, the XRD analysis revealed the fact that the entrapment was not good enough:

– at functionalized samples set, CI increases with the decreasing of the crystallites nanoparticles;
– in case of the non-functionalized linen fibrous supports, there is a proportional increasing of CI with the augmentation of nanoparticles size.
– The differential scanning calorimetry (DSC) also revealed higher enthalpy value compared to the reference one. The synthesized nanocomposites revealed higher thermal stability and higher enthalpy value compared to the reference one. In the meantime, MMT having a higher thermal conductivity as well as a greater heat capacity value, absorbed the heat transmitted from the surroundings and retarded the direct thermal impact to the polymer backbone.

Chemical composition and crystallinity of the studied samples influenced the thermal degradation behavior of the supports studied. Thus, a very much lower amount of carbonyl groups is found in the linen–ZnO nanocomposite specimens, according to the FTIR spectra. FTIR spectra revealed the existence of zinc oxide and MMT.

– The perspective research will be oriented to a more improved technique of fixing the ZnO nanoparticles to add multifunctionality of the studied fibrous nanocomposites.

Acknowledgements This study is financially supported by POSDRU 89/1.5/S/49944 and 59410 EURODOC (Doctoral Scholarships for Performance at European Level Research belonging both to "Gh.Asachi" Technical University and "Al.I.Cuza" University of Iasi, Romania.

References

1. Corrales T, Catalina F, Peinado C, Allen NS, Fontan E. Photooxidative and thermal degradation of polyethylenes interrelationship by chemiluminescence, thermal gravimetric analysis and FTIR data. J Photochem Photobiol A. 2002;147:213–24.
2. Gawas UB, Verenkar VMS, Mojumdar SC. Synthesis and characterization of $Co_{0.8}Zn_{0.2}Fe_2O_4$ nanoparticles. J Therm Anal Calorim. 2011;104:879–83.
3. Gonsalves LR, Mojumdar SC, Verenkar VMS. Synthesis and characterization of $Co_{0.8}Zn_{0.2}Fe_2O_4$ nanoparticles. J Therm Anal Calorim. 2011;104:869–73.
4. Gonsalves LR, Mojumdar SC, Verenkar VMS. Synthesis of cobalt nickel ferrite nanoparticles via autocatalytic decomposition of the precursor. J Therm Anal Calorim. 2010;100:789–92.
5. Gawas UB, Mojumdar SC, Verenkar VMS. Synthesis of cobalt nickel ferrite nanoparticles via autocatalytic decomposition of the precursor. J Therm Anal Calorim. 2010;100:867–71.
6. Verdu J, Rychly J, Audouin L. Synergism between polymer antioxidants - kinetic modelling. Polym Degrad Stab. 2003;79:503–9.
7. Allen NS, Edge M, Corrales T, Childs A, Liauw CM, Catalina F, et al. Ageing and stabilization of filled polymers: an overview. Polym Degrad Stab. 1998;61:183–99.
8. Mojumdar SC, Moresoli C, Simon LC, Legge RL. Edible wheat gluten (WG) protein films: preparation, thermal, mechanical and spectral properties. J Therm Anal Calorim. 2011;104:929–36.
9. Gawas UB, Mojumdar SC, Verenkar VMS. $Ni_{0.5}Mn_{0.1}Zn_{0.4}Fe_2(C_4H_2O_4)_3{\cdot}6N_2H_4$ precursor and $Ni_{0.5}Mn_{0.1}Zn_{0.4}Fe_2O_4$ nanoparticle. Preparation, IR spectral, XRD, SEM-EDS and thermal analysis. J Therm Anal Calorim. 2009;96:49–52.
10. Mocanu AM, Odochian L, Apostolescu N. TG-FTIR study on thermal degradation in air of some new diazoaminoderivatives. J Thermal Anal Calorim. 2010;100(2):615–22.
11. Singhal M, Chhabra V, Kang P, Shah DO. Synthesis of ZnO nanoparticles for varistor application using Zn-substituted aerosol OT microemulsion. Mater Res Bull. 1997;32:239–47.
12. Hingorani S, Pillai V, Kumar P, Multani MS, Shah DO. Microemulsion mediated synthesis of zinc-oxide nanoparticles for varistor studies. Mater Res Bull. 1993;28:1303–10.
13. Fan Q, John J, Ugbolue SC, Wilson AR, Dar YS, Yang Y. Nanoclay-modified polypropylene dyeable with acid and disperse dyes. AATCC Rev. 2003;3(6):25.
14. Chen CG, Khobaib M, Curliss D. Epoxy layered silicate nanocomposites. Prog Org Coat. 2003;47:376–83.
15. Xu T, Xie CS. Characterization of the dispersion of tetrapod-like nano-ZnO whiskers in acrylic resin and properties of the nano-composite coating system. Prog Org Coat. 2003;46:297–301.
16. Patscheider J, Zehnder T, Diserens M. Structure–performance relations in nanocomposite coatings. Surf Coat Technol. 2001;146–147:201–8.
17. Song L, Hu Y, Wang S, Fan W, Chen Z. A study on the synthesis and properties of polyurethane/clay nanocomposites. Int J Polym Anal Charact. 2003;8(5):317.
18. Mani G, Fan Q, Ugbolue SC, Eiff IM. Effect of nanoparticle size and its distribution on the dyeability of polypropylene. AATCC Rev. 2003;3(1):22.
19. White LA, Bertoniere NR. Preparation of cotton/clay nanocomposites. Polymer. 2002;43(2):1279.
20. Stretz HA, Koo JH, Dimas VM, Zhang Y. Flame retardant properties of polycarbonate/montmorillonite clay nanocomposite blends. Polymer. 2001;42(2):50.
21. Reuscher H, Hinsenkorn R. BETA W7 MCT-new ways in surface modification. J Incl Phenom Macrocycl. 1996;25:191–6.

22. Ogata N, Ogawa T, Ida T, Yanagawa T, Ogihara T, Yamashita A. Structure and thermal/mechanical properties of drawn Nylon-6 hybrid. Sen'i Gakkaishi. 1995;51(9):439.
23. Patterson A. The Scherrer formula for X-ray particle size determination. Phys Rev. 1939;56(10):978–82.
24. Xiao-Juan J, Pascal Kamdem D. Chemical composition crystallinity and crystallite cellulose size in populus hybrids and aspen. Cellul Chem Technol. 2009;43(7–8):229–34.
25. Tserki V, Zafeiropoulo NE, Simon F, Panayiotou C. A study of the effect of acetylation and propionylation surface treatments on natural fibres. J Appl Sci Manuf. 2005;36:1110.
26. Park, S et al.: Biotechnology B for biofuels http://www.biotechnologyforbiofuels.com/content/3/1/10 (2010) 3:10.
27. Jiang Z-H, Zhong Y, So C-L, Hse C-Y. Rapid prediction of wood crystallinity in *Pinus elliotii* plantation wood by near-infrared spectroscopy. J Wood Sci. 2007;53:449–453.
28. Garvey CJ, Parker IH, Simon GP. On the interpretation of X-ray diffraction powder patterns in terms of the nanostructure of cellulose I fibres. Macromol Chem Phys. 2005;206:1568–75.
29. Mwalkambo LY, Ansell MP. Chemical modification of hemp, sisal, jute, and kapok fibers by alkalization. J Appl Polym Sci. 2002;84:2222.
30. Ye DY, Farriol X. Preparation and characterization of methylcellulose from *Miscanthus sinensis*. Cellulose. 2005;12:507.
31. Revola JF, Dietricha NDD, Goring AI. Effect of mercerization on the crystallite size and crystallinity index in cellulose from different sources. Can J Chem. 1987;65:1724.
32. Nevell TP, Zeronian SH, editors. Cellulose chemistry and its applications. Chichester: Ellis Horwood Ltd.; 1985. p. 423–54.
33. Lee HJ, Yeo SY, Jeong SH. Antibacterial effect of nanosized silver colloidal solution on textile fabrics. J Mater Sci. 2003;38:2199–204.
34. Riva A, Algaba IM, Montserrat P. Action of a finishing product in the improvement of the ultraviolet protection provided by cotton fabrics. Modelisation of the effect. Cellulose. 2006;13:697–704.